*J. Fluid Mech.* (1967), *vol.* 30, *part* 1, *pp.* 83–95
*Printed in Great Britain*



# The magnetohydrodynamic thrust bearing

By E. ROLAND MAKI, DENNIS C. KUZMA
Research Laboratories, General Motors Corporation, Warren, Michigan 48090
AND RUSSELL J. DONNELLY
University of Chicago, Illinois 60637†

(Received 16 March 1967)

The magnetohydrodynamic lubrication flow in a step-type thrust bearing has been investigated both theoretically and experimentally. The experimental configuration consisted of nine identical segments arranged on a circular plate. Flow was induced by rotating the upper plate. Pressures, voltages and torques were recorded. Provision was made for passing current radially through the segments, and it was shown that the torque could be reduced to zero and even reversed by this means. Good agreement has been obtained between the analysis and the experimental results.

## 1. Introduction

This paper is the third in a series in which we have investigated some experimental flow configurations relevant to the theory of magnetohydrodynamic lubrication. The first paper (Kuzma, Maki & Donnelly 1964) dealt with the magnetohydrodynamic squeeze film, and contained the first experimental data on this subject. The second paper (Maki, Kuzma & Donnelly 1966) described a magnetohydrodynamic externally pressurized thrust bearing. Both the first and second papers contained analyses which, when fluid inertia effects were included, agreed well with experiment. One can feel confident that some progress has been made toward understanding these radial Hartmann flow problems. Related treatments have been given by Krieger, Day & Hughes (1966) for the thrust bearing, and Dudzinsky, Young & Hughes (1966) for the journal bearing.

The present paper describes a different class of configuration: magnetohydrodynamic lubrication flow in a self-acting step-type thrust bearing. It will be shown experimentally that the torque on this type of bearing may be reduced to zero by proper application of a current across the bearing. An analytical investigation of a step slider bearing has been carried out by Hughes (1963). His analysis was done in rectangular co-ordinates for a single-step slider, while the present analysis is done in cylindrical co-ordinates for a multiple-step bearing. The results of the experiment are in good agreement with the theory.

† Now at the Department of Physics, University of Oregon, Eugene, Oregon 97403.

## 2. Apparatus and procedure

*Construction*

A simplified sketch of the apparatus is shown in figure 1. The step geometry is machined in the lower plate and consists of nine equally spaced segments. Each segment is composed of an entry region, a step region, and a minimum clearance region. The entry regions have an average film thickness of 0·0194 in. and the step regions have an average film thickness of 0·0123 in. The separation of the plates at the minimum clearance regions averaged 0·007 in. Twenty-four

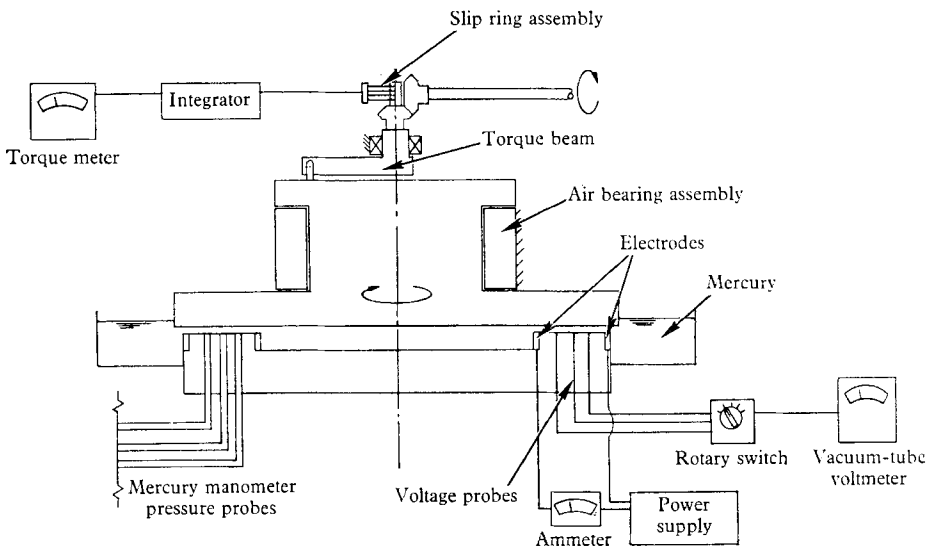


FIGURE 1. Simplified drawing of apparatus.

manometer pressure openings and a similar number of voltage probes are distributed among the nine segments on the lower plate to form the pattern shown in figure 2. The voltage probes are held in place with epoxy adhesive and machined flat with the various surfaces on which they are located. Ring electrodes are located on the inner and outer edges of the step region, and are connected to a direct current power supply. The top plate is flat and is the upper boundary of the clearance space. Both plates were made of plastic and all metal components in contact with the mercury were made of stainless steel. A photograph of a segment of the lower plate is shown in figure 3, plate 1.

Separation of the plates is adjustable and is set by shims. This separation is maintained at the desired value by a pressurized gas bearing which provides a low friction support for the top plate. The top plate is rotated about a vertical axis by a variable speed mechanical drive through a series of cog belts and mitre gears. A cantilever beam instrumented with strain gauges is the final connexion from the drive system to the top plate assembly. Because frictional losses in gas bearings are negligible the strain beam can be used to measure the torque acting on the top plate via the mercury film. A small slip ring assembly transfers signals from the rotating strain beam to the torque meter.

The mercury is contained in a pan encircling the top and bottom plates. As shown in figure 4, plate 2, the pan has a diameter considerably larger than the plates to eliminate any container influence on the film and the mercury level is maintained at a level somewhat higher than the plate separation to ensure that air would not be drawn into the clearance space. There is also a mercury reservoir located in the depression which forms the centre of the lower plate.

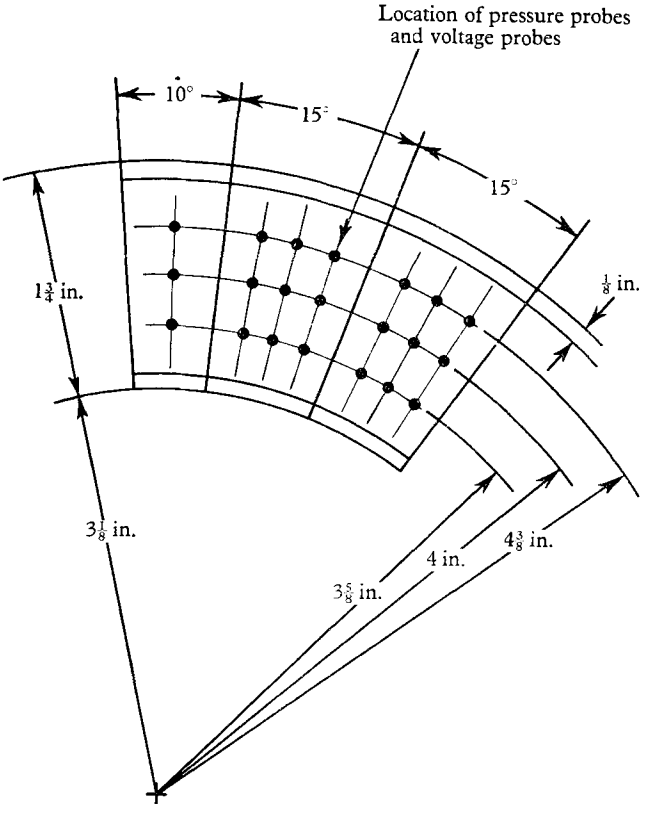


FIGURE 2. Pressure opening and voltage probe location.

The magnet was that of the 32·5 in. cyclotron at the University of Chicago. This magnet can produce a field of 16,000 G homogeneous to about 0·1 % in the region of the apparatus. Vertical spacing between the pole pieces of this magnet is 8·75 in.

*Instrumentation*

Pressures at points in the lubricating film and the inner and outer reservoirs were read from glass capillary tube manometers. In figure 4, plate 2, a photograph of the apparatus shows these manometers in the upper background. The manometer scale consisted of a sheet of graph paper with millimeter divisions. Three of the pressure taps are duplicated to allow cross-checking of selected pressures. The voltage probes and the inner and outer electrodes are connected to a rotary switch shown at the left of figure 4 so that the output could be conveniently observed on one vacuum tube voltmeter. Three of the voltage probes were also duplicated.

The electrical signal from the strain beam was amplified and displayed on a meter that had previously been calibrated by loading the beam with dead weights. Under certain circumstances it was found advantageous to integrate this signal electrically so that an averaged signal was recorded on the torque meter. Electrode current was supplied by a direct current power supply with 0·01 % regulation. An ammeter with $\frac{1}{2}$ % accuracy was used to measure this current. Rotation was supplied by a tapered cone variable speed transmission. The rate of rotation was determined by a digital tachometer and displayed on an electric counter directly in revolutions per minute.

### *Procedure*

The mercury was cleaned by the processes described by Kuzma *et al.* (1964). The apparatus was thoroughly cleaned before assembly and the clearance between plates was set. On adding mercury to the apparatus, great care had to be taken to establish a continuous film of mercury between the plates and to clear the manometer tubes of all entrained air. A vacuum pump was of considerable assistance in this task. Verification of proper gas-bearing operation was established by a simple continuity check. If the check indicated infinite resistance across the gas-bearing clearance there was no contact occurring in the gas-bearing assembly.

At this point, the apparatus was carefully pushed into the magnet and levelled. Rotation of the top plate was started and the flow allowed to come to equilibrium at the appropriate magnetic field. The observation consisted of reading the manometers, the voltage taps, the electrode current and the torque. Readings without rotation or applied field were taken periodically to establish reference levels, to look for drifts, and to provide information on reproducibility. The lubricating film was examined regularly to ensure that it was continuous throughout the time data were being collected.

## 3. Experimental results

Experimental results are shown in figures 5 to 10, and are compared with the results of the analysis.

The relationship between torque and rate of rotation is shown in figure 5 for zero field and for 12·5 kG under open circuit conditions. The agreement between theory and experiment is best at low speeds and high magnetic field. The discrepancy is probably due to the neglect of fluid inertia effects in the theory.

The effect of passing current radially through the bearing is illustrated in figure 6. Here the torque is plotted as a function of total current through the bearing for two different speeds of rotation at 10 kG. The negative current means that the current flow is from the outer to the inner electrode. It can be seen that the torque on the bearing can be reduced to zero and even reversed. Excellent agreement is obtained between theory and experiment.

The open circuit voltage potential is shown in figure 7 as a function of radius for a field strength of 10·0 kG and a rotation rate of 60·2 rev/min. The agreement between theory and experiment is not good, and at the present time we have no

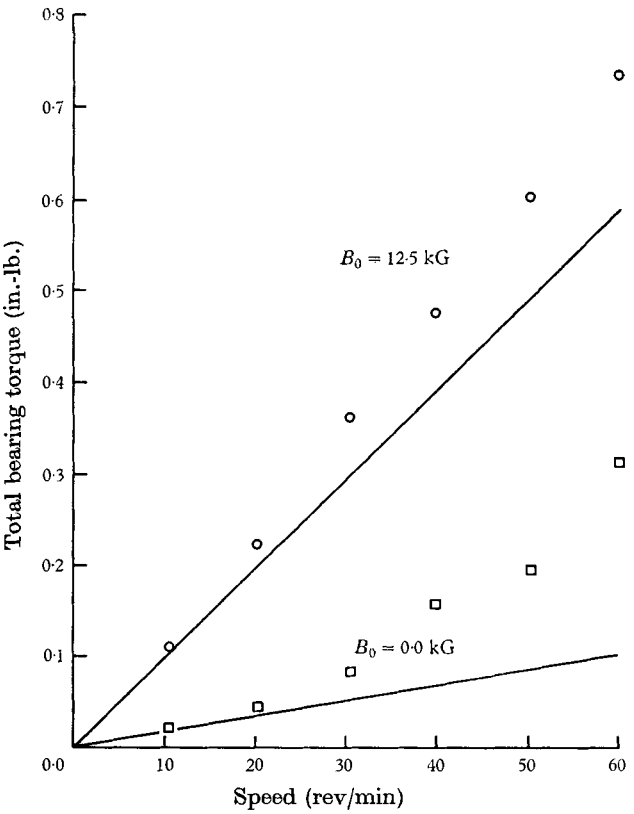


FIGURE 5. Total bearing torque versus speed for open circuit conditions.

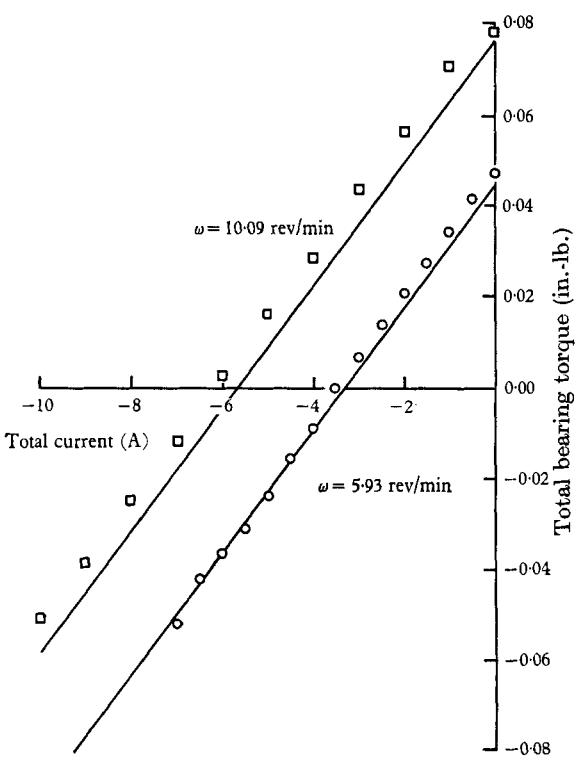


FIGURE 6. Total bearing torque versus total current at various speeds for a magnetic field strength of 10·0 kG.

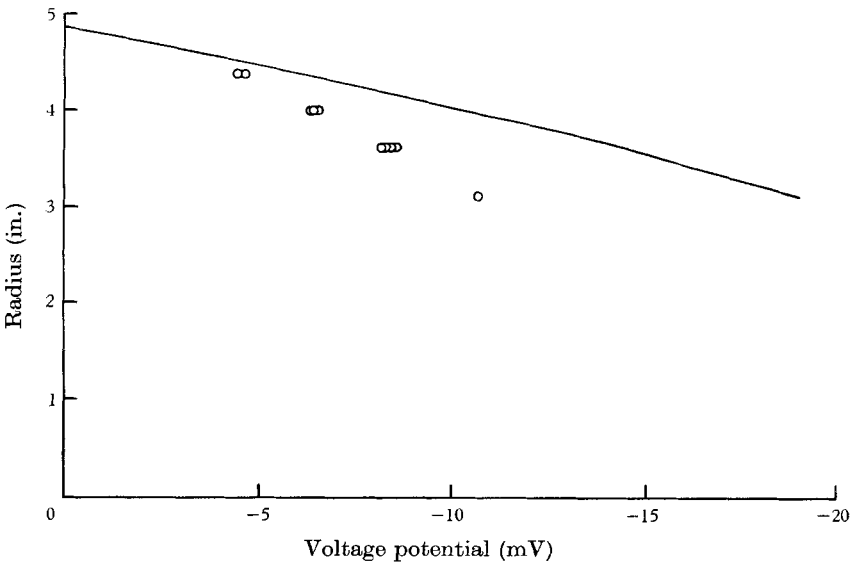


FIGURE 7. Open circuit voltage potential versus radius for a magnetic field strength of 10·0 kG and a speed of 60·2 rev/min.

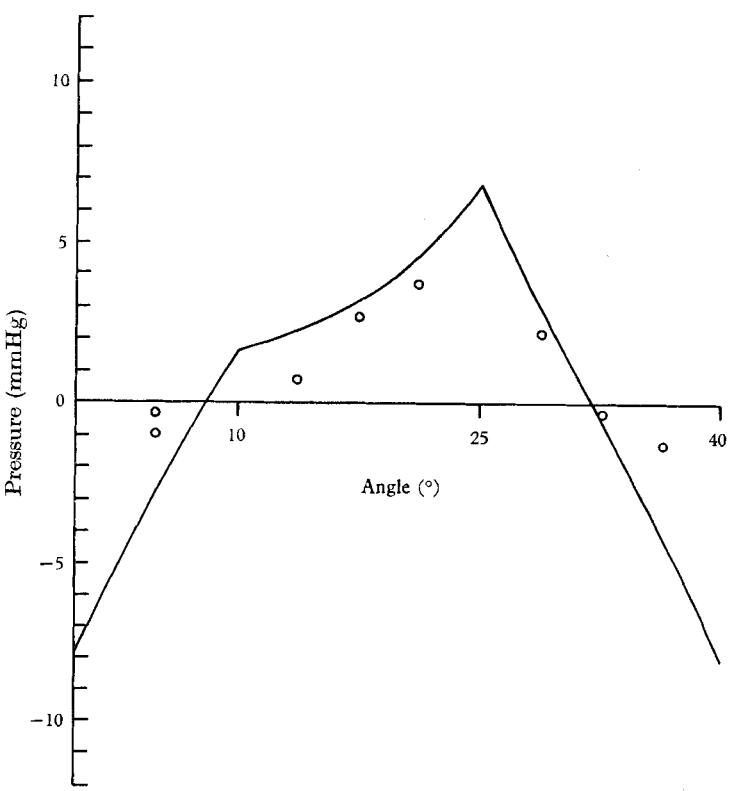


FIGURE 8. Open circuit pressure profiles for a magnetic field strenth of 12·5 kG and a speed of 30·0 rev/min at a radius of 4·0 in.

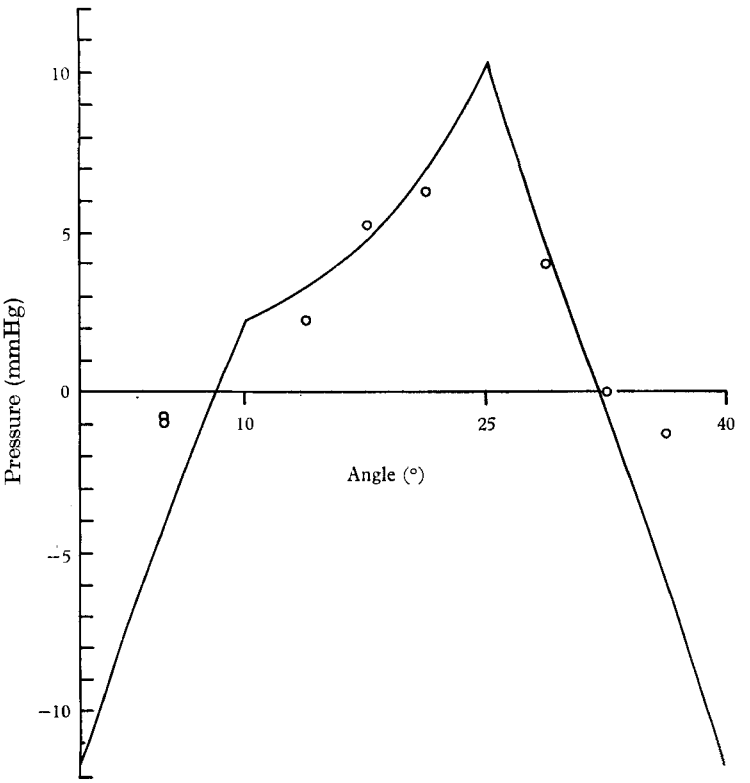


FIGURE 9. Open circuit pressure profiles for a magnetic field strength of 10·0 kG and a speed of 60·2 rev/min at a radius of 4·0 in.

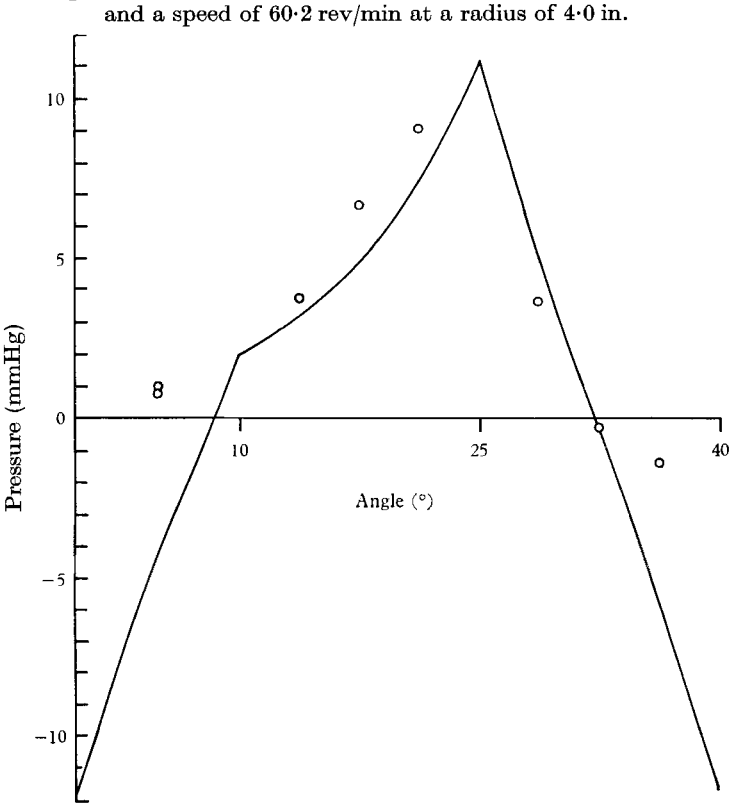


FIGURE 10. Open circuit pressure profiles for a magnetic field strength of 7·5 kG and a speed of 90·03 rev/min at a radius of 4·0 in.

explanation for the discrepancy. There is, however, evidence from other hydromagnetic experiments at the University of Chicago that the boundary conditions between mercury and metals such as stainless steel and aluminium are not governed by the bulk conductivity (see, for example, III of Caldwell 1964). Surface layers may play an important role here. The experimental results do show the assumption is justified that the voltage potential is a function of radius only.

Pressure profiles along the step are shown in figures 8–10 for various speeds of rotation and magnetic field strengths under open circuit conditions. All the pressure profiles shown were taken at a radius of 4·0 in. In order to correct partially for centrifugal force, the experimental points have been reduced by the amount $P_c \ln r/r_1$, where $P_c$ is the measured pressure difference between inner and outer radii. The agreement between theory and experiment is fairly good in all cases. Discrepancies are probably due to small deviations in the steps and possibly to fluid inertia effects as well.

## 4. Analysis

The analysis for the magnetohydrodynamic lubrication flow in a finite-step slider bearing has been given by Hughes (1963). In order to interpret the results of the present experiment, we shall use a similar method of analysis.

The equation of conservation of momentum in hydromagnetics is

$$\rho(\mathbf{u}.\nabla)\,\mathbf{u} = -\nabla p + \mu\nabla^2\mathbf{u} + \sigma\mathbf{J}\times\mathbf{B} \tag{1}$$

where $\rho$ is density, $\mathbf{u}$ is velocity, $p$ is pressure, $\mu$ is viscosity, $\sigma$ is electrical conductivity, $\mathbf{J}$ is current density, and $\mathbf{B}$ is magnetic field strength. If the usual assumptions of magnetohydrodynamic lubrication theory are used, the momentum equations become

$$-\frac{\partial p}{\partial r} + \mu\frac{\partial^2 u_r}{\partial z^2} + J_\theta B_0 = 0, \tag{2}$$

$$-\frac{1}{r}\frac{\partial p}{\partial \theta} + \mu\frac{\partial^2 u_\theta}{\partial z^2} - J_r B_0 = 0, \tag{3}$$

where $B_0$ is the applied magnetic field in the $z$ direction.

If the applied voltage is assumed to be a function of $r$ only, Ohm's law becomes

$$J_r = \sigma(E_r + u_\theta B_0), \tag{4}$$

$$J_\theta = -\sigma u_r B_0, \tag{5}$$

where $\mathbf{E}$ is the electric field intensity. Equations (2) and (3) then become

$$\frac{\partial^2 u_r}{\partial z^2} - \left(\frac{M}{h}\right)^2 u_r = \frac{1}{\mu}\frac{\partial p}{\partial r}, \tag{6}$$

$$\frac{\partial^2 u_\theta}{\partial z^2} - \left(\frac{M}{h}\right)^2 u_\theta = \frac{1}{\mu r}\frac{\partial p}{\partial \theta} + \frac{M}{h}\sqrt{\frac{\sigma}{\mu}}E_r, \tag{7}$$

where

$$M = B_0 h(\sigma/\mu)^{\frac{1}{2}} \tag{8}$$

and $h$ is the thickness of the fluid film. The boundary conditions are

$$z = 0, \quad u_r = 0, \quad u_\theta = r\omega; \tag{9}$$

$$z = h, \quad u_r = 0, \quad u_\theta = 0. \tag{10}$$

Since $p$ is assumed to be a function of $r$ and $\theta$ only, equations (6) and (7) may be solved directly to give

$$u_r = -\frac{h^2}{M^2}\frac{1}{\mu}\frac{\partial p}{\partial r}\left[1 - \frac{\cosh\left(Mz/h - \frac{1}{2}M\right)}{\cosh \frac{1}{2}M}\right], \tag{11}$$

$$u_\theta = -\frac{h^2}{M^2}\left(\frac{1}{\mu r}\frac{\partial p}{\partial \theta} + \frac{M}{h}\left(\frac{\sigma}{\mu}\right)^{\frac{1}{2}} E_r\right)\left[1 - \frac{\cosh\left(Mz/h - \frac{1}{2}M\right)}{\cosh \frac{1}{2}M}\right] + r\omega \frac{\sinh\left(M - Mz/h\right)}{\sinh M}. \tag{12}$$

From continuity

$$\frac{\partial}{\partial r}\left(r\int_0^h u_r\, dz\right) + \frac{\partial}{\partial \theta}\left(\int_0^h u_\theta\, dz\right) = 0. \tag{13}$$

If the expressions for velocity are substituted into equation (13) we obtain

$$r\frac{\partial}{\partial r}\left(r\frac{\partial p}{\partial r}\right) + \frac{\partial^2 p}{\partial \theta^2} = 0. \tag{14}$$

The boundary conditions on $p$ are

$$p(r_1, \theta) = p(r_2, \theta) = 0. \tag{15}$$

Since the pressure must be continuous at the interface of each bearing section, we obtain:
when $0 \leqslant \theta \leqslant \theta_1$

$$p = \sum_1^\infty \sin\left(\alpha_n \ln r/r_1\right)\left[a_n \sinh \alpha_n \theta \sinh \alpha_n(\theta_2 - \theta_1) + b_n \cosh \alpha_n \theta \sinh \alpha_n(\theta_2 - \theta_1)\right], \tag{16}$$

when $\theta_1 \leqslant \theta \leqslant \theta_2$

$$p = \sum_1^\infty \sin\left(\alpha_n \ln r/r_1\right)\left[a_n \sinh \alpha_n(\theta_2 - \theta) \sinh \alpha_n \theta_1 + b_n \sinh \alpha_n(\theta_2 - \theta) \cosh \alpha_n \theta_1 + c_n \sinh \alpha_n(\theta - \theta_1) \sinh \alpha_n(\theta_3 - \theta_2) + b_n \sinh \alpha_n(\theta - \theta_1) \cosh \alpha_n(\theta_3 - \theta_2)\right], \tag{17}$$

when $\theta_2 \leqslant \theta \leqslant \theta_3$

$$p = \sum_1^\infty \sin\left(\alpha_n \ln r/r_1\right)\left[c_n \sinh \alpha_n(\theta_3 - \theta) \sinh \alpha_n(\theta_2 - \theta_1) + b_n \cosh \alpha_n(\theta_3 - \theta) \sinh \alpha_n(\theta_2 - \theta_1)\right], \tag{18}$$

where

$$\alpha_n = n\pi/\ln\left(r_2/r_1\right). \tag{19}$$

For each bearing segment

$$I_s = \int_0^{\theta_s}\int_0^h r J_r\, dz\, d\theta. \tag{20}$$

Thus $$I_s = \frac{\sigma B_0}{\mu}\{[p(r,\theta_1)-p(r,0)]f_1+[p(r,\theta_2)-p(r,\theta_1)]f_2 + [p(r,\theta_3)-p(r,\theta_2)]f_3\}+2\sigma r E_r h g_1/M+\sigma B_0 r^2\omega g_1 h/M, \tag{21}$$

where $$f_n = \frac{2h_n^3}{M_n^3}\tanh\tfrac{1}{2}M_n - \frac{h_n^3}{M_n^2} \tag{22}$$

and $$g_1 = \theta_1\tanh\tfrac{1}{2}M_1+(\theta_2-\theta_1)\tanh\tfrac{1}{2}M_2+(\theta_3-\theta_2)\tanh\tfrac{1}{2}M_3. \tag{23}$$

Equation (21) may be rearranged to give

$$E_r = \frac{I_s M}{2\sigma g_1 h r}-\frac{B_0 r\omega}{2}-\frac{B_0 M}{2\mu r h g_1} \times\{[p(r,\theta_1)-p(r,0)]f_1+[p(r,\theta_2)-p(r,\theta_1)]f_2+[p(r,\theta_3)-p(r,\theta_2)]f_3\}. \tag{24}$$

The second boundary condition for the pressure requires that $Q_\theta$ is continuous across the interface between bearing regions where

$$Q_\theta = \int_0^h u_\theta\, dz, \tag{25}$$

or $$Q_\theta = \left(\frac{1}{\mu r}\frac{\partial p}{\partial\theta}+\frac{M}{h}\left(\frac{\sigma}{\mu}\right)^{\frac{1}{2}}E_r\right)\left(\frac{2h^3}{M^3}\tanh\tfrac{1}{2}M-\frac{h^3}{M^2}\right)+r\omega\frac{h}{M}\tanh\tfrac{1}{2}M. \tag{26}$$

The value for $E_r$ may be substituted into (26). The boundary conditions for continuity of flow may then be applied. When use is made of the orthogonality relations

$$\int_0^1 \sin m\pi x\sin n\pi x\,\alpha x \begin{matrix} = 0 & (m\neq n)\\ = \tfrac{1}{2} & (m=n)\end{matrix} \tag{27}$$

we obtain $$\begin{vmatrix} d_n^{11} & d_n^{12} & d_n^{13}\\ d_n^{21} & d_n^{22} & d_n^{23}\\ d_n^{31} & d_n^{32} & d_n^{33}\end{vmatrix}\begin{vmatrix} a_n\\ b_n\\ c_n\end{vmatrix} = \begin{vmatrix} e_n^1\\ e_n^2\\ e_n^3\end{vmatrix}, \tag{28}$$

where the values for the matrices $D_n$ and $E_n$ are given in the appendix.

Equation (28) may be solved to give

$$\begin{vmatrix} a_n\\ b_n\\ c_n\end{vmatrix} = D_n^{-1}E_n. \tag{29}$$

The pressure is then determined by using the values for $a_n$, $b_n$ and $c_n$ in equations (16), (17) and (18). Only the first ten terms in the series have been used in the analysis.

The voltage potential is determined by integrating the electric field strength.

$$\phi = -\int_r^{r_2} E_r\, dr, \tag{30}$$

$$\phi = -\frac{I_s M}{2\sigma h g_1}\ln r_2/r-\frac{B_0\omega}{4}(r_2^2-r^2) -\frac{B_0 M\ln r_2/r_1}{2\mu h g_1}\sum_1^\infty\left\{\left[\frac{(-1)^n-\cos\dfrac{n\pi\ln r/r_1}{\ln r_2/r_1}}{n\pi}\right]\right.$$

$$\times [a_n(f_1-f_2)\sinh\alpha_n(\theta_2-\theta_1)\sinh\alpha_n\theta_1 + b_n(f_1-f_2)\sinh\alpha_n(\theta_2-\theta_1)\cosh\alpha_n\theta_1 + b_n(f_3-f_1)\sinh\alpha_n(\theta_2-\theta_1) + b_n(f_2-f_3)\sinh\alpha_n(\theta_2-\theta_1)\cosh\alpha_n(\theta_3-\theta_2) + c_n(f_2-f_3)\sinh\alpha_n(\theta_2-\theta_1)\sinh\alpha_n(\theta_3-\theta_2)]\Big\}. \tag{31}$$

The torque per bearing segment is given by

$$T_s = \mu\int_{r_1}^{r_2}\int_0^{\theta_s} r^2\frac{\partial u_\theta(r,\theta,0)}{\partial z}\,d\theta\,dr, \tag{32}$$

$$T_s = -\frac{I_s B_0}{4}(r_2^2-r_1^2)+\frac{r_2^4-r_1^4}{4}\left(\frac{B_0\omega(\sigma\mu)^{\frac{1}{2}}g_1}{2}+\frac{\mu\omega M g_2}{h}\right) + \sum_1^\infty\left\langle\left[-n\pi\ln r_2/r_1\frac{(-1)^n r_2^2-r_1^2}{4\ln^2 r_2/r_1+n^2\pi^2}\right]\sinh\alpha_n(\theta_2-\theta_1)\right. \left\{\left(\frac{a^2f_1}{2}-\frac{h_1}{M_1}\tanh\tfrac{1}{2}M_1\right)[a_n\sinh\alpha_n\theta_1+b_n(\cosh\alpha_n\theta_1-1)] + \left(\frac{a^2f_2}{2}-\frac{h_2}{M_2}\tanh\tfrac{1}{2}M_2\right)[c_n\sinh\alpha_n(\theta_3-\theta_2)+b_n\cosh\alpha_n(\theta_3-\theta_2) - a_n\sinh\alpha_n\theta_1-b_n\cosh\alpha_n\theta_1] + \left(\frac{a^2f_3}{2}-\frac{h_3}{M_3}\tanh\tfrac{1}{2}M_3\right)[-c_n\sinh\alpha_n(\theta_3-\theta_2)+b_n-b_n\cosh\alpha_n(\theta_3-\theta_2)]\right\}\Big\rangle, \tag{33}$$

where

$$g_2 = \theta_1\coth M_1+(\theta_2-\theta_1)\coth M_2+(\theta_3-\theta_2)\coth M_3. \tag{34}$$

We are indebted to Mr E. F. Bundshuh who prepared the drawings for the apparatus and Mr R. J. Buit who assisted with the assembly. Construction of the apparatus was carried out by Mr J. V. Radostitz and Mr M. Kowalczyk. Mr R. W. Koster prepared the mercury and assisted in all parts of the experiment. The research of R. J. Donnelly is supported by a grant from the National Science Foundation, NSF GP-2693, and by the Air Force Office of Scientific Research, Office of Aerospace Research, United States Air Force, under grant AF-AFOSR-785-65.

## Appendix

The values for the determinants $D_n$ and $E_n$ are given below:

$$d_n^{11} = -\frac{1}{2\mu}\alpha_n f_1\sinh\alpha_n(\theta_2-\theta_1) - \frac{M^3}{4\mu g_1 h^3}(f_3-f_1)(f_1-f_2)\sinh\alpha_n(\theta_2-\theta_1)\sinh\alpha_n\theta_1,$$

$$d_n^{12} = -\frac{M^3}{4\mu g_1 h^3}[(f_3-f_1)(f_1-f_2)\sinh\alpha_n(\theta_2-\theta_1)\cosh\alpha_n\theta_1 + (f_3-f_1)^2\sinh\alpha_n(\theta_2-\theta_1) + (f_3-f_1)(f_2-f_3)\sinh\alpha_n(\theta_2-\theta_1)\cosh\alpha_n(\theta_3-\theta_2)],$$

$$d_n^{13} = -\frac{1}{2\mu}\alpha_n f_3 \sinh\alpha_n(\theta_2-\theta_1)$$
$$-\frac{M^3}{4\mu g_1 h^3}(f_3-f_1)(f_2-f_3)\sinh\alpha_n(\theta_2-\theta_1)\sinh\alpha_n(\theta_3-\theta_2),$$

$$d_n^{21} = -\frac{1}{2\mu}\alpha_n f_2 \cosh\alpha_n(\theta_2-\theta_1)\sinh\alpha_n\theta_1$$
$$-\frac{1}{2\mu}\alpha_n f_1 \sinh\alpha_n(\theta_2-\theta_1)\cosh\alpha_n\theta_1$$
$$-\frac{M^3}{4\mu g_1 h^3}(f_2-f_1)(f_1-f_2)\sinh\alpha_n(\theta_2-\theta_1)\sinh\alpha_n\theta_1,$$

$$d^{22} = -\frac{1}{2\mu}\alpha_n f_2 \cosh\alpha_n(\theta_2-\theta_1)\cosh\alpha_n\theta_1$$
$$+\frac{1}{2\mu}\alpha_n f_2 \cosh\alpha_n(\theta_3-\theta_2)$$
$$-\frac{1}{2\mu}\alpha_n f_1 \sinh\alpha_n(\theta_2-\theta_1)\sinh\alpha_n\theta_1$$
$$-\frac{M^3}{4\mu g_1 h^3}[(f_2-f_1)(f_1-f_2)\sinh\alpha_n(\theta_2-\theta_1)\cosh\alpha_n\theta_1$$
$$+(f_2-f_1)(f_3-f_1)\sinh\alpha_n(\theta_2-\theta_1)$$
$$+(f_2-f_1)(f_2-f_3)\sinh\alpha_n(\theta_2-\theta_1)\cosh\alpha_n(\theta_3-\theta_2)],$$

$$d_n^{23} = \frac{1}{2\mu}\alpha_n f_2 \sinh\alpha_n(\theta_3-\theta_2)$$
$$-\frac{M^3}{4\mu g_1 h^3}(f_2-f_1)(f_2-f_3)\sinh\alpha_n(\theta_2-\theta_1)\sinh\alpha_n(\theta_3-\theta_2),$$

$$d_n^{31} = \frac{1}{2\mu}\alpha_n f_2 \sinh\alpha_n\theta_1$$
$$-\frac{M^3}{4\mu g_1 h^3}(f_3-f_2)(f_1-f_2)\sinh\alpha_n(\theta_2-\theta_1)\sinh\alpha_n\theta_1,$$

$$d_n^{32} = -\frac{1}{2\mu}\alpha_n f_3 \sinh\alpha_n(\theta_2-\theta_1)\sinh\alpha_n(\theta_3-\theta_2)$$
$$+\frac{1}{2\mu}\alpha_n f_2 \cosh\alpha_n\theta_1$$
$$-\frac{1}{2\mu}\alpha_n f_2 \cosh\alpha_n(\theta_2-\theta_1)\cosh\alpha_n(\theta_3-\theta_2)$$
$$-\frac{M^3}{4\mu g_1 h^3}[(f_3-f_2)(f_1-f_2)\sinh\alpha_n(\theta_2-\theta_1)\cosh\alpha_n\theta_1$$
$$+(f_3-f_2)(f_3-f_1)\sinh\alpha_n(\theta_2-\theta_1)$$
$$+(f_3-f_2)(f_2-f_3)\sinh\alpha_n(\theta_2-\theta_1)\cosh\alpha_n(\theta_3-\theta_2)],$$

$$d_n^{33} = -\frac{1}{2\mu}\alpha_n f_3 \sinh\alpha_n(\theta_2-\theta_1)\cosh\alpha_n(\theta_3-\theta_2)$$
$$-\frac{1}{2\mu}\alpha_n f_2 \sinh\alpha_n(\theta_3-\theta_2)\cosh\alpha_n(\theta_2-\theta_1)$$
$$-\frac{M^3}{4\mu g_1 h^3}(f_3-f_2)(f_2-f_3)\sinh\alpha_n(\theta_2-\theta_1)\sinh\alpha_n(\theta_3-\theta_2),$$

$$e_n^1 = \left(\frac{\sigma}{\mu}\right)^{\frac{1}{2}}\frac{M^2}{h^2}\frac{I_s}{2\sigma g_1}(f_3-f_1)\left\{\frac{1}{n\pi}[(-1)^n-1]\right\}$$
$$-\frac{M^2\omega}{2h^2}(f_3-f_1)\left[n\pi\frac{(-1)^n r_2^2-r_1^2}{4\ln^2(r_2/r_1)+n^2\pi^2}\right]$$
$$+\frac{\omega h}{M}(\tanh\tfrac{1}{2}M_3-\tanh\tfrac{1}{2}M_1)\left[n\pi\frac{(-1)^n r_2^2-r_1^2}{4\ln^2(r_2/r_1)+n^2\pi^2}\right],$$

$$e_n^2 = \left(\frac{\sigma}{\mu}\right)^{\frac{1}{2}}\frac{M^2}{h^2}\frac{I_s}{2\sigma g_1}(f_2-f_1)\left\{\frac{1}{n\pi}[(-1)^n-1]\right\}$$
$$-\frac{M^2\omega}{2h^2}(f_2-f_1)\left[n\pi\frac{(-1)^n r_2^2+r_1^2}{4\ln^2(r_2/r_1)+n^2\pi^2}\right]$$
$$+\frac{\omega h}{M}(\tanh\tfrac{1}{2}M_2-\tanh\tfrac{1}{2}M_1)\left[n\pi\frac{(-1)^n r_2^2-r_1^2}{4\ln^2(r_2/r_1)+n^2\pi^2}\right],$$

$$e_n^3 = \left(\frac{\sigma}{\mu}\right)^{\frac{1}{2}}\frac{M^2}{h^2}\frac{I_s}{2\sigma g_1}(f_3-f_2)\left\{\frac{1}{n\pi}[(-1)^n-1]\right\}$$
$$-\frac{M^2\omega}{2h^2}(f_3-f_2)\left[n\pi\frac{(-1)^n r_2^2-r_1^2}{4\ln^2(r_2/r_1)+n^2\pi^2}\right]$$
$$+\frac{\omega h}{M}(\tanh\tfrac{1}{2}M_3-\tanh\tfrac{1}{2}M_2)\left[n\pi\frac{(-1)^n r_2^2-r_1^2}{4\ln^2(r_2/r_1)+n^2\pi^2}\right].$$

## REFERENCES


CALDWELL, D. R. 1964 *Phys. Fluids*, **7**, 1338.

DUDZINSKY, S. J., YOUNG, F. J. & HUGHES, W. F. 1966 (To be published).

HUGHES, W. F. 1963 *Trans. ASME, Ser.* D, **85**, 129.

KRIEGER, R. J., DAY, H. J. & HUGHES, W. F. 1966 *ASME Paper* 66 Lub. S-8. (To be published.)

KUZMA, D. C., MAKI, E. R. & DONNELLY, R. J. 1964 *J. Fluid Mech.* **19**, 395.

MAKI, E. R., KUZMA, D. C. & DONNELLY, R. J. 1966 *J. Fluid Mech.* **26**, 537.

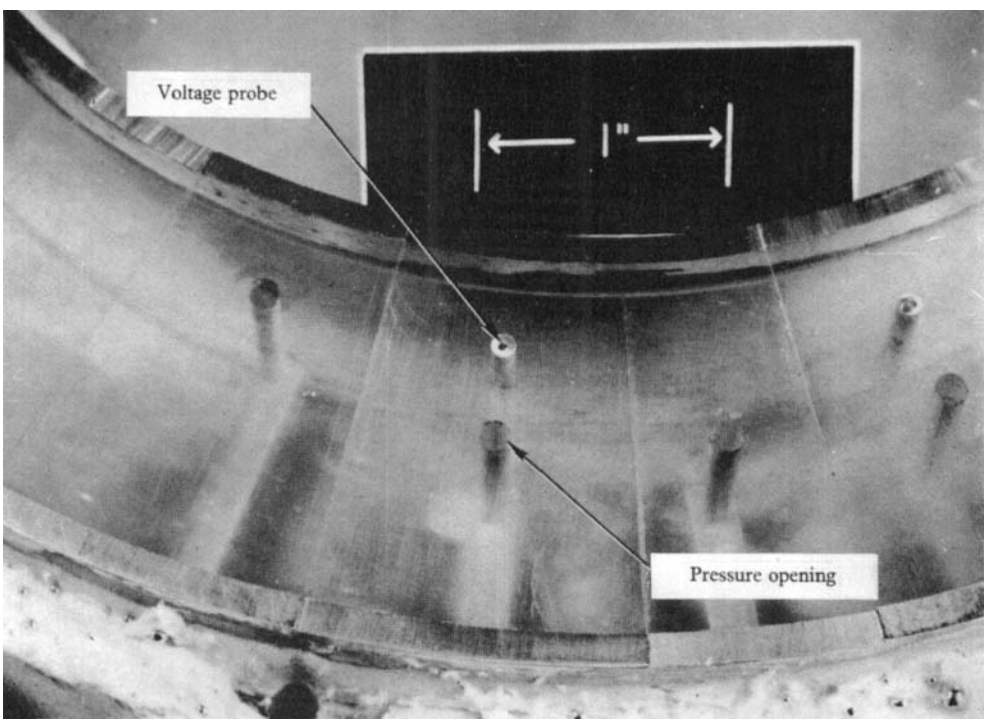


FIGURE 3. Photograph of step region.

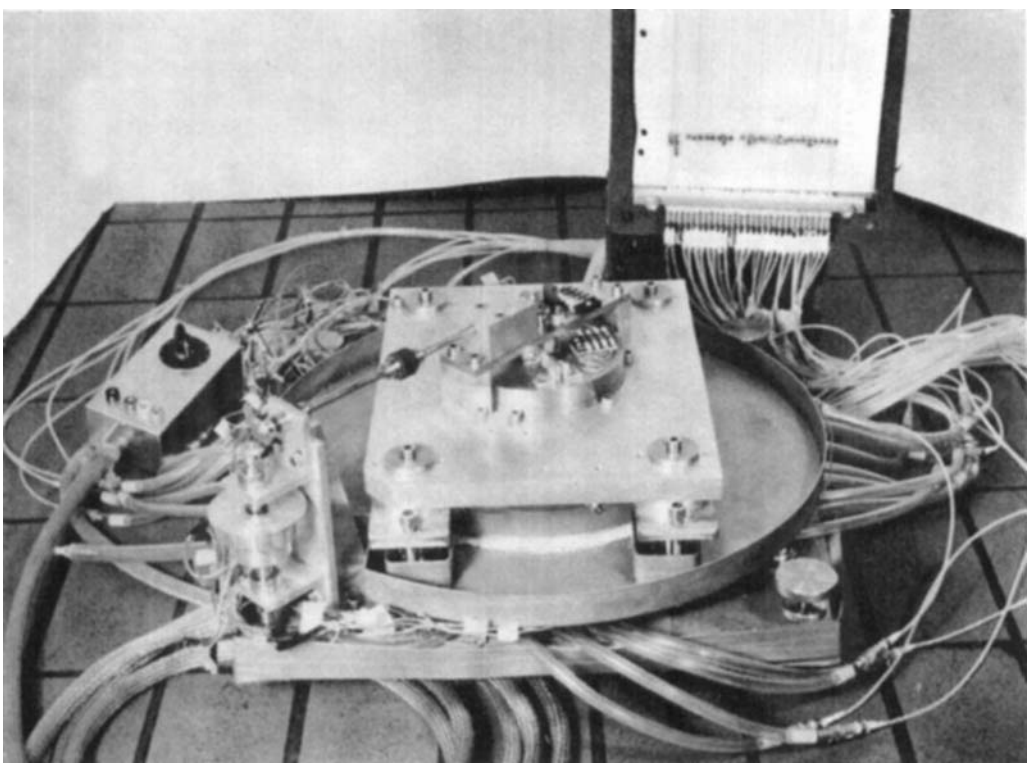

FIGURE 4. Photograph of apparatus removed from magnet.